Available online at www.sciencedirect.com
ScienceDirect
Journal of the European Ceramic Society 31 (2011) 1573–1580
www.elsevier.com/locate/jeurceramsoc

Preparation of aluminium lanthanum oxyapatite tapes, $La_{10}AlSi_5O_{26.5}$, by tape casting and reaction sintering

Isabel Santacruz*, José M. Porras-Vázquez, Enrique R. Losilla, Miguel A.G. Aranda

Departamento de Química Inorgánica, Cristalografía y Mineralogía, Universidad de Málaga, 29071 Málaga, Spain

Received 23 December 2010; received in revised form 4 March 2011; accepted 14 March 2011
Available online 9 April 2011

Abstract

Lanthanum apatite is one of the most promising materials as an electrolyte for intermediate-temperature solid oxide fuel cells (IT-SOFCs) which operate close to 700 °C. Here, we report the preparation and optimization of dense $La_{10}AlSi_5O_{26.5}$ tapes obtained by the combination of tape casting technology and reaction sintering. Homogeneous concentrated mixed suspensions of La_2O_3, Al_2O_3 and SiO_2 were prepared in ethanol. The effect of the solid loading, the binder content, ultrasound and the initial particle size of the materials onto the characteristics of the tapes (cracking, composition, microstructure and electrical properties) has been studied. This study paves the way for further improvement in the processing of oxyapatite electrolyte for solid oxide fuel cells.

Keywords: Tape casting; Electrical properties; Ionic conductivity; Apatite; Fuel cells

1. Introduction

Reduction of operating temperature of solid oxide fuel cells (SOFCs) down to intermediate temperature (600–800 °C) displays significant advantages such as lower working costs, improve the lifetime of the system and a decrease in the price for the interconnector materials. Oxy-apatites have high potential to be used as oxide ion conductors working at moderate temperatures (∼700 °C) for IT-SOFCs due to the presence of large conduction channels containing interstitial oxide ions.[1–4]

Different routes have been reported in the literature to prepare oxy-apatites such as solid state reaction,[5] sol–gel,[6] hot-pressing techniques,[7] mechano-syntheses,[8] precipitate method combined with an azeotropic-distillation process,[9] freeze–drying,[10] plasma spraying[11] or gel-casting.[12] All these synthesis routes show advantages and disadvantages. For example, the sol–gel technique implies several heating steps to promote the formation of a gel and ensure the removal of all the organic components. Mechanochemical synthesis needs long milling times (higher than 9 h) of the starting mixture.[13] In addition, both processes require a wide knowledge of the synthesis parameters to control the formation of important amounts of secondary phases. Materials prepared by freeze–drying can show significant uptake under wet atmospheres and this has effects on their structures and properties.[10] A comparative study[14] in the preparation of oxy-apatites by three different methods, conventional, spark plasma, and reaction sintering (RS) indicated that the latter led to pellets with the highest overall oxide ion conductivity.

Electrolytes to be used in SOFCs have to show high densities and thin thicknesses. In this way, oxy-apatite tapes and coatings have been recently prepared by tape casting,[15–17] plasma spraying[18] and sputtering.[19] Tape casting is a low-cost well established technique for manufacturing self-supporting ceramic sheets with a wide range of thicknesses (50–500 μm) in a continuous way, and has been generally used for the fabrication of microelectronic components.[20] The control of the colloidal properties of the suspensions is a critical step, and the key role of the additives is well known.[21,22] The suspensions need to show high stability, optimised viscosity for high shear stress and high solid loading for obtaining uniform sheets with high strength and sufficient flexibility for handling in the green state.

This work deals with the preparation and optimization of $La_{10}AlSi_5O_{26.5}$ tapes obtained by the combination of tape casting and reaction sintering. We have selected this composition because Al-doping allows a slightly lower sintering temperature maintaining the high ionic conductivity and transport

* Corresponding author. Tel.: +34 952 13 1992; fax: +34 952 13 1870.
E-mail address: isantacruz@uma.es (I. Santacruz).

0955-2219/$ – see front matter © 2011 Elsevier Ltd. All rights reserved.
doi:10.1016/j.jeurceramsoc.2011.03.023

Table 1
Properties of the studied suspensions.

Primary particle size	Initial suspension solid loading wt%/vol%/vol.fraction	BP content/wt%							
		η (18 s^{-1})/mPa s				η (100 s^{-1})/mPa s			
		0	10	20	30	0	10	20	30
Micro	45/13.5/0.135	3	–	–	–	2	–	–	–
	60/22/0.22	68	–	–	–	20	–	–	–
	70/31/0.31	510	1083	9150	–	130	1018	–	–
	73/34/0.34	640	1530	–	–	170	1556	–	–
Micro–Nano	22/5/0.05	210	–	–	–	50	–	–	–
	40/11/0.11	1515	2075	–	2760	280	377	–	807
	45/13.5/0.135	3030	–	–	–	570	–	–	–
Nano	22/5/0.05	650	–	–	–	142	–	–	–

number.[23] In an initial work,[24] we reported the preparation of $La_{10}AlSi_5O_{26.5}$ pellets by colloidal processing of diluted mixed suspensions of La_2O_3, Al_2O_3 and SiO_2, combined with die pressing and reactive sintering. Here, cheaper raw materials have been used (La_2O_3) and concentrated suspensions were prepared in ethanol to fabricate continuous $La_{10}AlSi_5O_{26.5}$ tapes. The effect of the solid loading, the binder system content, the use of ultrasound and the initial particle size of the materials onto the characteristics of the suspensions and tapes (cracking, composition, microstructure and electrical properties) has been studied.

2. Experimental

2.1. Processing conditions

$La_{10}AlSi_5O_{26.5}$ samples were prepared by reaction sintering using high purity oxides: micron powders of La_2O_3 (99.99%, Sigma–Aldrich, Steinheim, Germany), γ-Al_2O_3 (99.997%, Alfa Aesar, MA, USA) and SiO_2 (quartz, ABCR, 99.8%, ABCR, Karlsruhe, Germany). Nanosized powders of SiO_2 (Aeroxide 200, Degussa Evonik, Hanau, Germany) and γ-Al_2O_3 (Degussa, Aeroxide Alu C, Degussa Evonik, Hanau, Germany) were also used. Lanthanum oxide decarbonation was achieved by heating it at 1000 °C for 2 h. The powders were characterized in terms of particle/agglomerate size by scanning electron microscopy, SEM (JEOL SM 840, Tokyo, Japan) and transmission electron microscopy, TEM (JEOL 2000FX, Tokyo, Japan).

Diluted suspensions, 0.1 wt% solid content, of every powder were prepared in dried absolute ethanol (99.7% grade, Panreac, Barcelona, Spain) and optimised using different quantities of a polymeric dispersant (Hypermer KD6, Uniqema, Wirrall, UK), 0–3.0 wt% on a dry solid basis. The zeta potentials of those diluted suspensions were measured by microelectrophoresis (Zetasizer NanoZS, Malvern Instruments, Malvern, UK).

Concentrated mixed suspensions with the stoichiometric relations of oxides and the optimum amount of deflocculant were prepared in dried absolute ethanol. The effect of the particle size of the initial powder was studied by comparing suspensions with micron Al_2O_3 and SiO_2 powders (called Micro in the text), only nanosized Al_2O_3 and SiO_2 powders (called Nano in the text) or combination of both particle sizes in a ratio of 50/50 for each powder (called Micro–Nano in the text). In all cases, calcined micron La_2O_3 powder was used. Concentrated suspensions were prepared by mechanical stirring at different solid loadings—(i) Micro: 45, 60, 70 and 73 wt% (13.5, 22, 31, and 34 vol%, respectively), (ii) Micro–Nano: 22, 40 and 45 wt% (5, 11 and 13.5 vol%, respectively) and (iii) Nano: 22 wt% (5 vol%). A value of 5.262 g cm^3 was used as theoretical density of the mixture of powders.

The so-prepared suspensions (50 mL) were ultrasonically homogenized using a 400 W sonication probe (UP400s Hielscher Ultrasonics GmbH, Stuttgart, Germany) for 2 min. Suspensions were cooled in an ice-water bath during ultrasonication in order to avoid excessive heating.

For preparing the tape casting suspensions, PVB, Poly(vinyl butyral) (Aldrich, St. Louis, USA) was used as binder (B), and BBP, Benzylbutyl-phthalate (Merck-Schuchardt, Hohenbrunn, Germany) was used as plasticizer (P). The binder system, BP, was added to the suspensions to a total content of 10, 20 and 30 wt% (called 10BP, 20BP and 30BP, respectively) on a dry solid basis using a relative binder/plasticizer (B/P) ratio of 1. Table 1 summarizes the suspensions studied in this work. The suspensions were milled (MM200, Retsch, Haan, Germany) with alumina balls for 30, 60 and 90 min with the addition of 10, 20 and 30 wt% BP, respectively. Note that the milling was performed in 15 min steps, with the suspension being at room temperature for 10 min between each milling in order to avoid excessive heating of the suspension.

The rheological behaviour of the slips without and with the binder system was studied using a rotational viscometer (Model VT550, Thermo Haake, Karlsruhe, Germany) with a coaxial cylinder sensor, MV DIN, provided with a solvent trap to reduce evaporation. Flow curves were obtained with controlled rate (CR) measurements using a three-stage measuring program with a linear increase in the shear rate from 0 to 200 s^{-1} in 300 s, a plateau at 200 s^{-1} for 120 s, and a further decrease to zero shear rate in 300 s. Before starting the rheological measurement the suspensions were presheared for 2 min at 50 s^{-1}.

Tape-casting experiments were carried out with a single blade system. Slips were cast onto a plastic film. The blade height was fixed at 550 μm and the casting speed at about 10 cm s^{-1}.

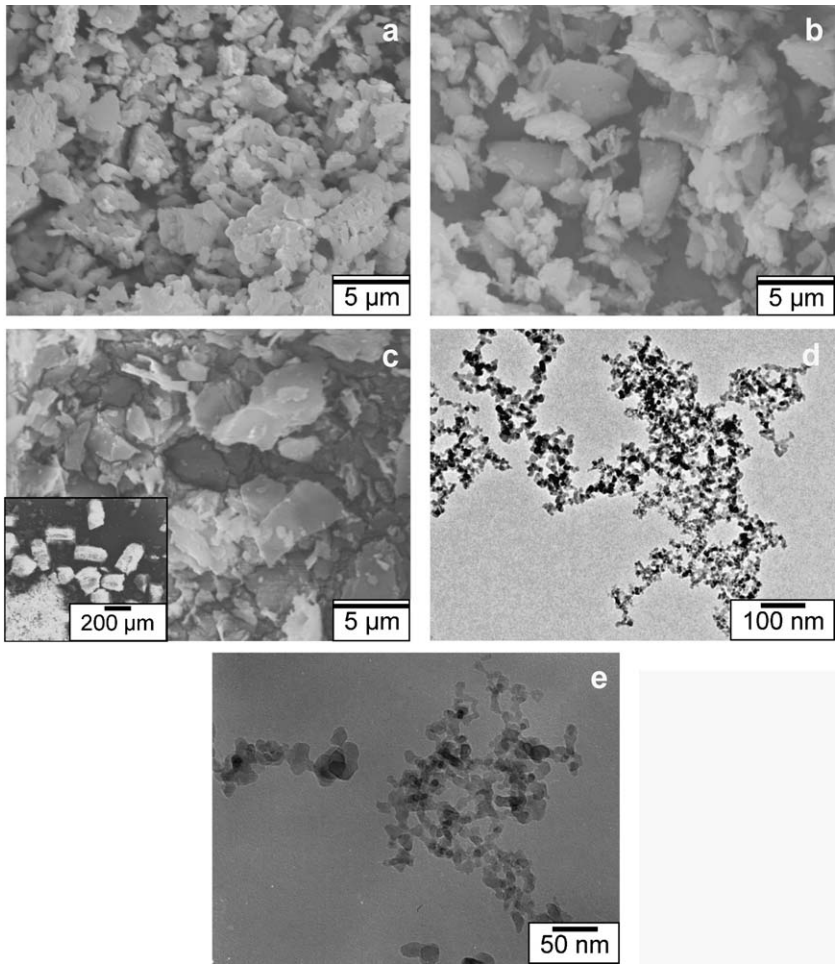

Fig. 1. Scanning electron micrographs of the starting micron powders: (a) La_2O_3, (b) SiO_2 and (c) Al_2O_3. Transmission electron micrographs of the nanosized powders: (d) SiO_2 and (e) Al_2O_3. The insets show a low magnification area.

Considering these parameters, the shearing of the suspension under the blade was calculated to be $\sim 18\,s^{-1}$. The tapes were dried at room temperature for 48 h. The thickness was measured by direct observation of the cross-section of the tapes by SEM. Organics were burned out from room temperature to 500 °C at 5 °C min^{-1} for 1 h. After this treatment, samples were heated at the same heating rate to a sintering temperature of 1120 °C and held for 2 h, then the furnace was heated up to the final target temperature of 1650 °C at the same heating rate before holding for 10 h. The porosity of the samples was estimated by SEM on cross-sections perpendicular to the casting direction.

2.2. Powder diffraction

Tapes were characterized by high resolution laboratory X-ray powder diffraction (LXRPD) at room temperature. Powder patterns were collected on a Philips X'Pert Pro MPD diffractometer equipped with a Ge(1 1 1) primary monochromator (strictly monochromatic $CuK_{\alpha 1}$ radiation) and an X'Celerator detector (PANalytical B.V., Almelo, Netherlands). The overall measurement time was ~4 h per pattern to have good statistics over the 2θ range of 10–130° with a 0.017° step size. Rietveld[25] analyses were carried out with the GSAS[26] suite of programs using the structural description reported previously for $La_{10}AlSi_5O_{26.5}$.[27]

2.3. Electrical characterisation

Electrodes were made by coating opposite sintered tape faces with METALOR® 6082 platinum paste and gradually heating to 950 °C at a rate of 10 °C min^{-1} in air to decompose the paste and harden the Pt residue. Successive treatments were made to achieve an electrical resistance of both tape faces lower than 1 Ω. Impedance data were collected using a Hewlett-Packard 4284A impedance analyzer over the frequency range 20 Hz to 1 MHz from 500 to 1000 °C. Measurement processes were electronically controlled by the winDETA package of programs.[28] The tapes were mounted in a home made alumina conductivity jig, with two Pt wires and were placed in a tubular furnace. Electrical data were taken every 25 °C. A delay time of 30 min at each temperature was selected to ensure thermal equilibrium. Temperatures were reproducible to ±1 °C.

3. Results and discussion

Fig. 1 shows the micrographs obtained by SEM and TEM for micron and nanosized reactive powders. In general, commercial micron powders (La_2O_3, SiO_2 and Al_2O_3) are agglomerated; micron-Al_2O_3 powders are also forming aggregates larger than

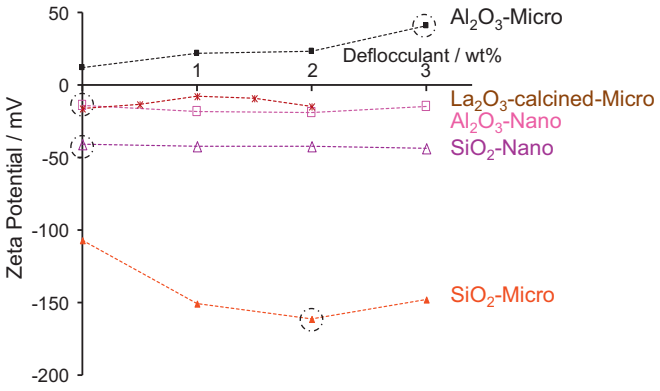

Fig. 2. Zeta potential values for every micron and nanosized reactive oxide as a function of deflocculant (KD6) weight.

100 μm. SiO_2 and Al_2O_3 nanosized powders show a primary particle size of 10–25 nm, as can be seen from the TEM micrographs (Fig. 1d and e). Physical characteristics of those powders, except La_2O_3 99.99%, are described elsewhere.[24] In the previous work,[24] a very high purity La_2O_3 powder, 99.999%, was used; however, in this work less pure and hence less expensive La_2O_3 powder has been used. The surface behaviour of both La_2O_3 powders was different when measured under the same conditions. Ultrapure La_2O_3 powder was charged positively and La_2O_3 powder used in this work was charged negatively, viz. 66 and −14 mV, respectively, after the addition of 2.0 wt% KD6. Fig. 2 shows the evolution of zeta potential values of every powder with the deflocculant content. All the powders show a negative zeta potential, except micron Al_2O_3. In this case, Al_2O_3 powders might be coated by the rest of the powders favouring the heterocoagulation process.[29] However, since the amount of Al_2O_3 present in the mixed suspensions is quite small, 2.5 wt% referred to the total powder amount, the contribution of the heterocoagulation process is likely not significant. The apparent pH of these diluted suspensions lies between 8 and 10. The best stabilization was obtained after the addition of 2.0 and 3.0 wt% KD6 for micron SiO_2 and Al_2O_3 powders, respectively, where maximum absolute zeta potential values were achieved, as it is marked in Fig. 2. For La_2O_3, nanosized SiO_2 and Al_2O_3 powders, no relevant zeta potential improvements were observed after the deflocculant addition, so no extra dispersant was added for the stabilization of the mixed suspension.

Concentrated mixed suspensions with the optimised deflocculant content were prepared at different solid loadings, and were studied through their rheological behaviours. Fig. 3a and b shows the evolution of the viscosity of 2 min ultrasonicated Micro, Micro–Nano and Nano suspensions with volume fraction at shear rates of 18 and 100 s^{-1}, respectively. The former corresponds to the casting rate. The viscosity values of those suspensions were taken from the up-curves. In general, suspensions show higher viscosity values at 18 s^{-1} rather than 100 s^{-1} which is related with a fluidificant behaviour (pseudoplastic or plastic). As expected, in all the suspensions, the viscosity increased exponentially with solids content. Nano suspensions were only measured at 5 vol% (22 wt%) since suspensions with higher solid contents were not homogeneous and became a gel,

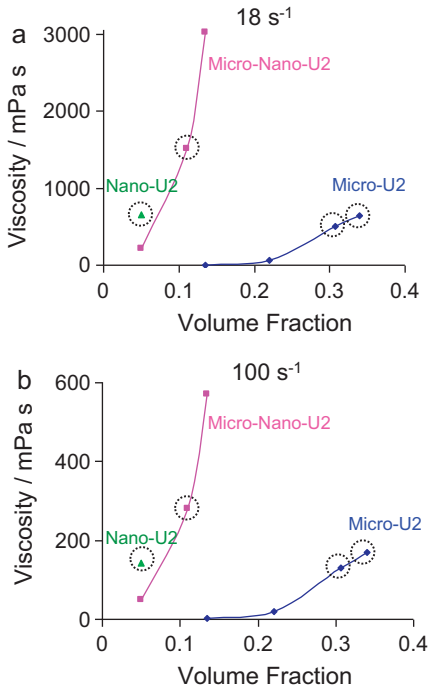

Fig. 3. Evolution of the viscosity with solids loading (volume fraction) of Micro, Micro–Nano and Nano suspensions at two shear rates of: (a) 18 s^{-1} and (b) 100 s^{-1}.

and lower solid contents were out of the scope of this study. 5 vol% Nano suspension displayed higher viscosity than the corresponding Micro–Nano suspension, viz. 142 and 50 mPa s, respectively at 100 s^{-1}. This is more dramatic when the shear rate is lower (e.g. 18 s^{-1}). Micro suspensions showed the lowest viscosity values, even at higher solid contents (e.g. 20 mPa s at 22 vol% measured at 100 s^{-1}). A compromise between solid content, viscosity and homogeneity is required for the preparation of the tapes. From these studies, solid contents of 11 and 5 vol% (40 and 22 wt%) were selected for Micro–Nano and Nano suspensions respectively, and 31 and 34 vol% (70 and 73 wt%, respectively) for Micro suspensions.

Fig. 4 shows the viscosity curves of selected Micro (M) (31 and 34 vol%), Micro–Nano (MN) (11 vol%) and Nano (N) (5 vol%) suspensions at different binder and plasticizer contents, without and with 2 min ultrasonication (U0, U2). The inset of Fig. 4a shows the viscosity curves of Micro suspensions without binders. The application of ultrasound decreases the viscosity of the Micro suspensions (31 vol%) providing better homogeneity. For Micro–Nano suspensions the viscosity increases slightly with the application of ultrasound due to the presence of nanosized powders; however, its application is required to obtained homogeneous samples, and longer or shorter ultrasound times led to inhomogeneous samples.[24] In general, suspensions show a shear thinning behaviour; however, 31 and 34 vol% Micro suspensions with 10 wt% binder content (M-31-U2-10BP and M-34-U2-10BP) show a near Newtonian behaviour (Fig. 4a). This might be related with the formation/destruction of structure/agglomerates during the measurement due to the presence of the binder system. Furthermore, the viscosity increases radically with the binder content, e.g. 31 vol% Micro suspensions

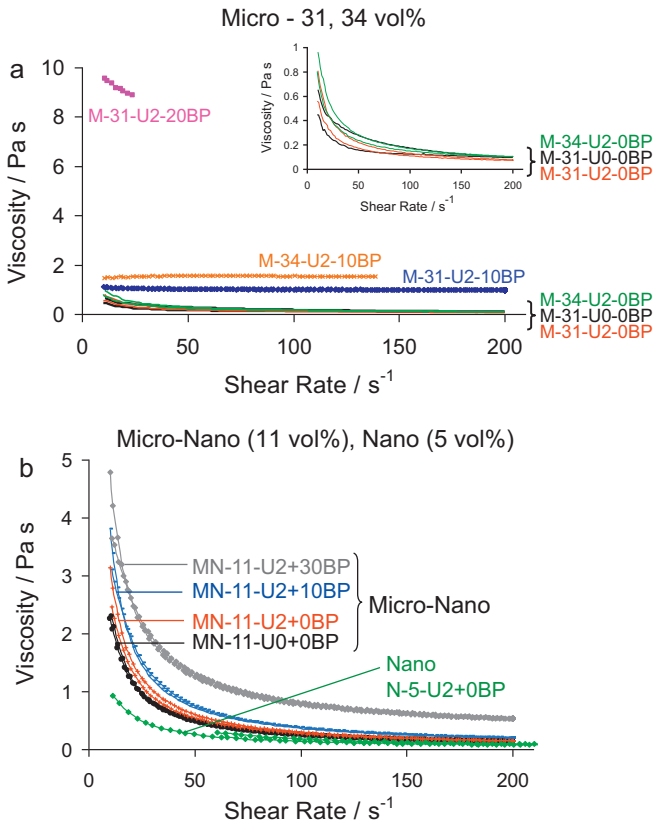

Fig. 4. Viscosity curves of selected suspensions: (a) Micro (31 and 34 vol%) and (b) Micro–Nano (11 vol%) and Nano (5 vol%), without and with 2 min ultrasonication (U0, U2) and different binder system contents. The inset shows the viscosity curves of the Micro suspensions without binders.

with 20 wt% BP (M-31-U2-20BP) show very high viscosity, ~9 Pa s at a shear rate of 18 s^{-1}, which was not able to be measured in all the range of shear rate. Fig. 4b shows also the effect of the BP content onto the rheological behaviour of 11 vol% Micro–Nano suspensions. All the suspensions used in the preparation of the tapes were 2 min ultrasonicated prior to the binder addition.

The effect of the primary particle size of the powders and the binder system content onto the green tapes is shown in Fig. 5. Fig. 5a shows a photograph of the green tape prepared from M-34-U2-10BP. Micro-tapes with higher binder content showed the same appearance. Fig. 5b and c shows tapes prepared from 11 vol%-Micro–Nano suspension with the addition of 30 wt% BP (MN-11-U2-30BP) and 5 vol% Nano suspension with 30 wt% BP (N-5-U2-30BP). All Micro–Nano tapes appeared completely cracked after drying; however, by increasing the BP content the tapes were less cracked. All the tapes prepared from 5 vol% Nano suspensions appeared cracked after drying. The effect of particle size plays a dramatic effect onto the tapes. Colloidally stable nanopowder suspensions are known to display a markedly lower volume loading at the same viscosity compared to suspensions with larger particle sizes.[30,31] The decrease in solid content with the particle size has an important effect onto the tapes (cracking). The quality of the green tapes is also related with the drying of the tapes. The drying process consists of two stages[22,32]; the first is controlled by capillary migration of the solvent, and the second is controlled by solvent diffusion through the solidified part of the film. In our case, a thin dried layer was formed just after the casting experiment on the upper surface of the tape, producing homogeneous tapes. The presence of this type of binders through the formation of a protective layer around the particles allows the dried green tapes to be manipulated and stored during weeks or even months without any reaction with the atmospheric water and carbon dioxide. Note this is an important issue since the green tapes contain La_2O_3 which is a reactive powder.

Tapes prepared from 31 vol% Micro suspensions with BP contents of 10 and 20 wt% (M-31-U2-10BP and M-31-U2-20BP) and 34 vol% Micro suspensions with BP contents of 10 and 20 wt% (M-34-U2-10 and M-34-U2-20) were selected for further studies as they showed the best appearance. Fig. 6 shows SEM micrographs of the cross-sections of selected green tapes, (a) M-31-U2-10BP, (b) M-31-U2-20BP, (c) M-34-U2-10BP and (d) M-34-U2-20BP. Homogeneous green tapes were obtained with thickness ranging 300–400 μm according to SEM measurements. Uniform and densely packed green microstructures without the presence of large binder agglomerates were observed, thus demonstrating that there was a suitable homogenization of the slips. The quality and flexibility of the tapes were high; because of this flexibility M-34-U2-10BP tape appeared slightly bended in the micrograph, Fig. 6c, so its real thickness is believed to be slightly larger than that shown there. The density of the green tapes prepared from 31 vol% suspensions increases by increasing the binder content, however, for 34 vol% tapes it decreases by increasing the BP amount. Further studies are needed to clarify this different behaviour. The same tendency on the density of the tapes is observed onto the sintered tapes (Fig. 7). From the micrographs it can be seen that homogeneous tapes with thickness ~200 μm were obtained after sintering.

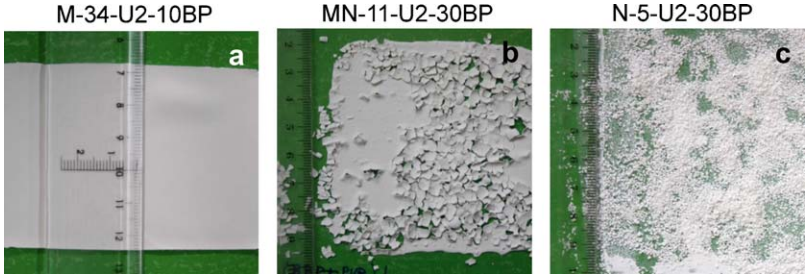

Fig. 5. Images of selected $La_{10}AlSi_5O_{26.5}$ green tapes: (a) M-34-U2-10BP, (b) MN-11-U2-30BP and (c) N-5-U2-30BP.

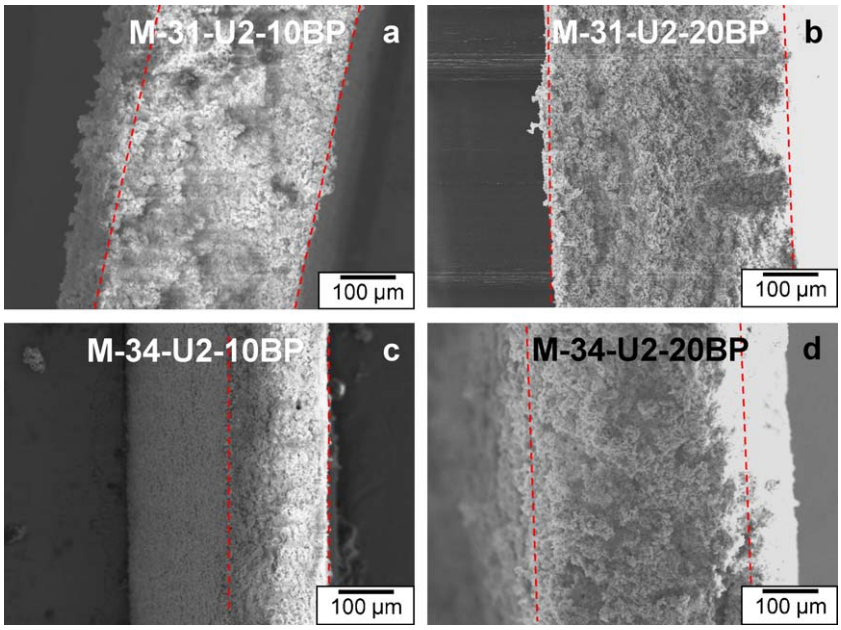

Fig. 6. Scanning electron micrographs (cross section) for $La_{10}AlSi_5O_{26.5}$ green tapes: (a) M-31-U2-10BP, (b) M-31-U2-20BP, (c) M-34-U2-10BP and (d) M-34-U2-20BP.

Table 2 summarizes the effect of binder system content onto the properties of the final samples prepared from the most concentrated Micro suspensions (34 vol%), i.e. compaction (percentage of theoretical density, %TD) and the presence of secondary phase, $LaAlO_3$. Dense tapes, 90–95% TD, were obtained from this concentrated suspension with the lowest amount of binders (M-34-U2-10BP) in agreement with Fig. 7c. Tapes with lower solid content showed lower den-

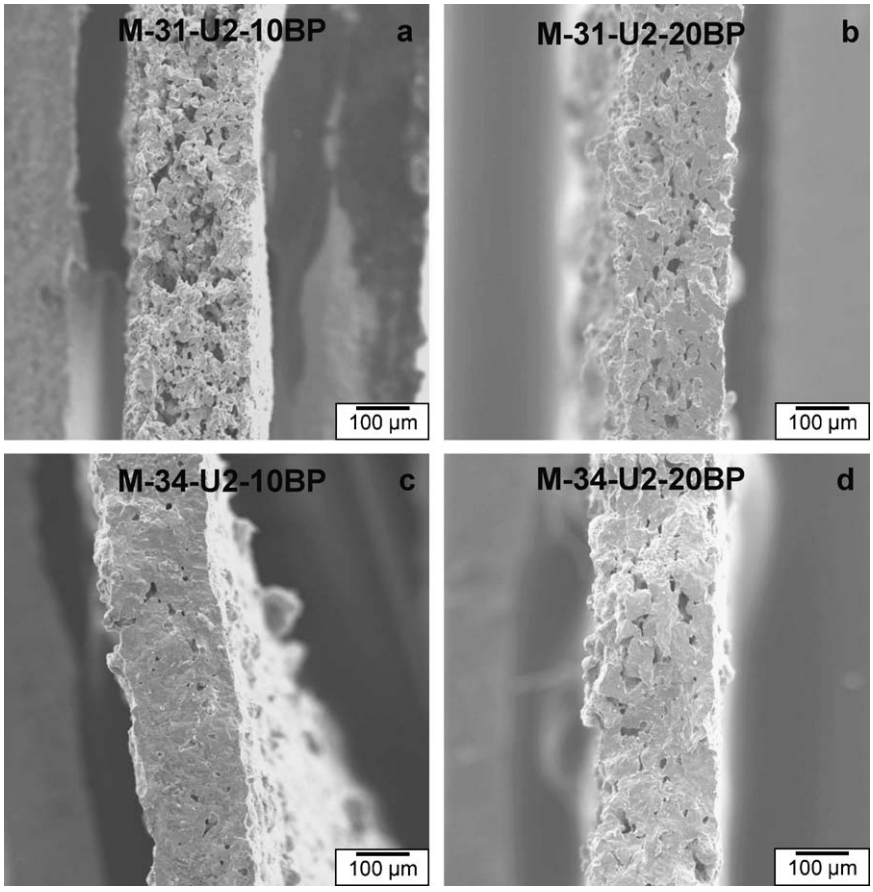

Fig. 7. Scanning electron micrographs (cross section) for $La_{10}AlSi_5O_{26.5}$ sintered tapes: (a) M-31-U2-10BP, (b) M-31-U2-20BP, (c) M-34-U2-10BP and (d) M-34-U2-20BP. (1120 °C/2 h–1650 °C/10 h).

Table 2
Properties of the tapes prepared from 34 vol% Micro suspensions.

Sample	Density %TD	Secondary phase: $LaAlO_3$ wt%	Cell parameters			σ_{700} (mS cm^{-1})
			a (Å)	c (Å)	V (Å^3)	
M-34-U2-10BP	90–95	–	9.7293(1)	7.2320(1)	592.87(2)	12
M-34-U2-20BP	88	0.5(1)	9.7293(1)	7.2317(1)	592.84(1)	6

sity values (≤85% TD), so those properties are not reported in Table 2.

Selected parts of the $La_{10}AlSi_5O_{26.5}$ tapes with the best properties (M-34-U2-10BP and M-34-U2-20BP), were grinded and their powder patterns were analyzed by the Rietveld method using the structural descriptions previously reported.[27] The occupation factors for lanthanum, silicon and aluminium sites were conveniently modified to describe the nominal stoichiometry. Only the overall parameters (histogram scale factor, background coefficients, unit cell parameters, zero-shift error, and peak shape pseudo-Voigt coefficients) and weight fractions of side phases (if necessary) were refined. Atomic parameters were not optimized. Final Rietveld figures of merit were good with R_F ranging between 3 and 4%; as an example of the refinement quality, the fit to the X-ray pattern of $La_{10}AlSi_5O_{26.5}$ for M-34-U2-20BP tape is shown in Fig. 8. The cell parameters (a, c and volume) of this oxyapatite are given in Table 2. The reported cell volumes published in the literature, prepared by reaction sintering, for $La_{10}AlSi_5O_{26.5}$ and $La_{10}Al_{0.5}Si_{5.5}O_{26.75}$ were 593.0 and 589.6 Å^3, respectively.[23] The close agreement between the unit cells for the tapes (see Table 2) and the reported values for bulk powders ensures the stoichiometry of our colloidal processed samples. The cell volume clearly indicates that the aluminium content in the tapes is higher than 0.80 per chemical formula.

Impedance spectroscopy was used to determine the electrical conductivity data for tapes with a relative density larger than 85% TD. Representative impedance data for M-34-U2-10BP at different temperatures are shown in Fig. 9. Similar plots were obtained for the remaining compositions. At low temperatures, i.e. 300 °C, a very complex spectrum formed by different overlapped contributions was observed. In this case it is difficult to determine separately the electrolyte and electrode responses by fitting with equivalent circuits. In the high temperature range,

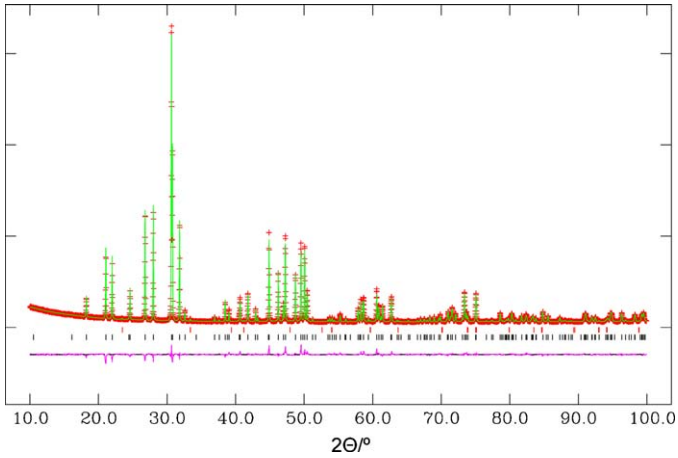

Fig. 8. Observed (crosses), calculated (full line), and difference curve (bottom) X-ray patterns for $La_{10}AlSi_5O_{26.5}$ sample from M-34-U2-20BP sintered tape.

the electrode response is dominant and overall conductivity was determined by the intercept of the impedance arc with the Z'-axis at high frequency. Total conductivity values at 700 °C were 12×10^{-3} and 6×10^{-3} S cm^{-1} for M-34-U2-10BP and M-34-U2-20BP, respectively. These results are very promising compared to those reported in literature for dense pellets[23,24] and more work in this way is under progress. Shaula et al.[23] reported a total conductivity value of 3×10^{-2} S cm^{-1} at 700 °C for pellets with the same composition (92%TD) using a dry reaction sintering methodology applying a final synthesis-sintering step of 1650 °C/10 h. At temperatures below 800 °C, M-34-U2-10BP tape shows higher conductivity values than YSZ. Similar conductivity values were reported by Bonhomme et al.[16] for a thick monolithic electrolyte sample prepared by laminated stacks from oxy-apatite powders ($La_9SrSi_6O_{26.5}$).

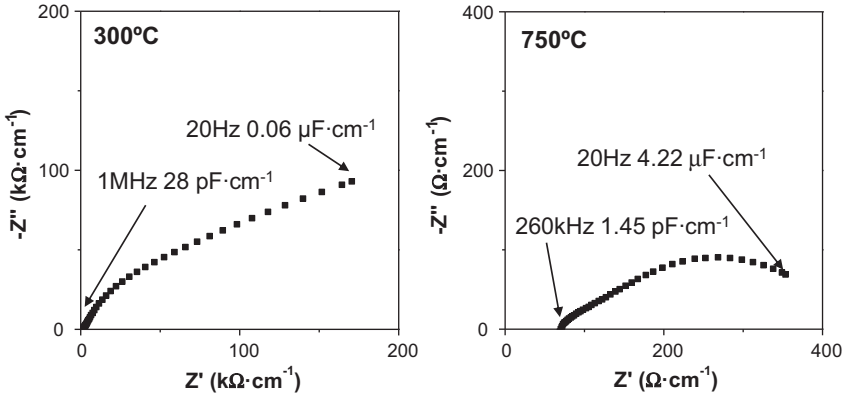

Fig. 9. Complex impedance plane plot at two temperatures for sintered M-34-U2-10BP tape. Selected frequency and capacitance points are highlighted.

4. Conclusions

Homogeneous dense $La_{10}AlSi_5O_{26.5}$ tapes were prepared by the combination of tape casting technology and reaction sintering. This combination exhibits economical advantages since tapes can be obtained in a continuous way and the final composition is obtained just in one step without long milling times required in other techniques, e.g. mechano-synthesis. Concentrated mixed suspensions of La_2O_3, Al_2O_3 and SiO_2 were prepared in ethanol. Different processing parameters were optimized, such as the initial powder size, the dispersant amount, the use of ultrasound and binder system content. Tapes with the desired composition, $La_{10}AlSi_5O_{26.5}$, density values of up to ~95% TD, thickness of ~200 μm and high conductivity values, 12×10^{-3} S cm^{-1} at 700 °C, were obtained in a single heating cycle.

Acknowledgements

This work has been supported by Spanish Ministry of Science and Innovation through project MAT2009-07016 and Ramón y Cajal fellowship (RYC-2008-03523) and Junta de Andalucía through project P10-FQM-6680. Authors thank Prof. Rodrigo Moreno's group (CSIC) for the use of Zetasizer NanoZS.

References

1. Panteix PJ, Julien I, Abélard P, Bernache-Assollant D. Influence of porosity on the electrical properties of $La_{9.33}(SiO_4)_6O_2$ oxy-apatite. *Ceram Int* 2008;**34**:1579–86.
2. Jiang P, Zhang L, He HQ, Yap RK, Xiang Y. Synthesis and characterization of lanthanum silicate apatite by gel-casting route as electrolytes for solid oxide fuel cells. *J Power Sources* 2009;**189**:972–81.
3. León-Reina L, Losilla ER, Martinez-Lara M, Bruque S, Aranda MAG. Interstitial oxygen conduction in lanthanum oxy-apatite electrolytes. *J Mater Chem* 2004;**14**:1142–9.
4. Marrero-López D, Martín-Sedeño MC, Peña-Martínez J, Ruiz-Morales JC, Núñez P, Aranda MAG, et al. Evaluation of apatite silicates as solid oxide fuel cell electrolytes. *J Power Sources* 2010;**195**:2496–506.
5. Shaula AL, Kharton VV, Waerenborgh JC, Rojas DP, Marques FMB. Oxygen ionic and electronic transport in apatite ceramics. *J Eur Ceram Soc* 2005;**25**:2583–6.
6. Jothinathan E, Vanmeensel K, Vleugels J, Van der Biest O. Powder synthesis, processing and characterization of lanthanum silicates for SOFC application. *J Alloys Compd* 2010;**495**:552–5.
7. Panteix PJ, Julien I, Bernache-Assollant D, Abelard P. Synthesis and characterization of oxide ion conductors with the apatite structure for intermediate temperature SOFC. *Mater Chem Phys* 2005;**95**:313–20.
8. Martínez-González LG, Rodríguez-Reyna E, Moreno KJ, Escalante-García JI, Fuentes AF. Ionic conductivity of apatite-type rare-earth silicates prepared by mechanical milling. *J Alloys Compd* 2009;**476**:710–4.
9. Yao HG, Wang JS, Hu DG, Li JF, Lu XR, Li ZJ. New approach to develop dense lanthanum silicate oxy-apatite sintered ceramics with high conductivity. *Solid State Ionics* 2010;**181**:41–7.
10. Marrero-López D, Martín-Sedeño MC, Ruiz-Morales JC, Núñez P, Ramos-Barrado JR. Preparation and characterisation of $La_{10-x}Ge_{5.5}Al_{0.5}O_{26-d}$ apatites by freeze-drying precursor method. *Mater Res Bull* 2010;**45**:409–15.
11. Gao W, Liao LHL, Coddet C. Plasma spray synthesis of $La_{10}(SiO_4)_6O_3$ as a new electrolyte for intermediate temperature solid oxide fuel cells. *J Power Sources* 2008;**179**:739–44.
12. Jiang SP, Zhang L, He HQ, Yap RK, Xiang Y. Synthesis and characterization of lanthanum silicate apatite by gel-casting route as electrolytes for solid oxide fuel cells. *J Power Sources* 2009;**189**:972–81.
13. Béchade E, Julien I, Iwata T, Masson O, Thomas P, Champion E, et al. Synthesis of lanthanum silicate oxyapatite materials as a solid oxide fuel cell electrolyte. *J Eur Ceram Soc* 2008;**28**:2717–24.
14. Porras-Vázquez JM, Losilla ER, León-Reina L, Marrero-López D, Aranda MAG. Microstructure and oxide ion conductivity in a dense $La_{9.33}(SiO_4)_6O_2$ oxy-apatite. *J Am Ceram Soc* 2009;**92**:1062–8.
15. Bonhomme C, Beaudet-Savignat S, Chartier T, Pirovano C, Vannier RN. Elaboration, by tape casting, and thermal characterization of a solid oxide fuel half-cell for low temperature applications. *Mater Res Bull* 2010;**45**:491–8.
16. Bonhomme C, Beaudet-Savignat S, Chartier T, Maître A, Sauvet AL, Soulestin B. Sintering kinetics and oxide ion conduction in Sr-doped apatite-type lanthanum silicates $La_9Sr_1Si_6O_{26.5}$. *Solid State Ionics* 2009;**180**:1593–8.
17. Bonhomme C, Beaudet-Savignat S, Chartier T, Geffroy PM, Sauvet AL. Evaluation of the $La_{0.75}Sr_{0.25}Mn_{0.8}Co_{0.2}O_{3-\delta}$ system as cathode material for ITSOFCs with $La_9Sr_1Si_6O_{26.5}$ apatite as electrolyte. *J Eur Ceram Soc* 2009;**29**:1781–8.
18. Dru S, Meillot E, Wittmann-Teneze K, Benoit R, Saboungi ML. Plasma spraying of lanthanum silicate electrolytes for intermediate temperature solid oxide fuel cells (ITSOFCs). *Surf Coat Technol* 2010;**205**:1060–4.
19. Ma CY, Briois P, Böhlmark J, Lapostolle F, Billard A. $La_{9.33}Si_6O_{26}$ electrolyte thin films for IT-SOFC application deposited by a HIPIMS/DC hybrid magnetron sputtering process. *Ionics* 2008;**14**:471–6.
20. Mistler RE. Tape casting—the basic process for meeting the needs of the electronics industry. *Am Ceram Soc Bull* 1990;**69**:1022–6.
21. Moreno R. The role of slip additives in tape-casting technology: Part I—solvents and dispersants. *Am Ceram Soc Bull* 1992;**71**:1521–30.
22. Lewis JA, Blackman KA, Ogden AL, Payne JA, Francies LF. Rheological properties and stress development during drying of tape-cast ceramic layers. *J Am Ceram Soc* 1996;**79**:3225–34.
23. Shaula AL, Kharton VV, Marques FMB. Oxygen ionic and electronic transport in apatite-type $La_{10-x}(Si\ Al)_6O_{26\pm\delta}$. *J Solid State Chem* 2005;**178**:2050–61.
24. Santacruz I, Porras-Vázquez JM, Losilla ER, Nieto MI, Moreno R, Aranda MAG. Colloidal processing and characterization of aluminium-doped lanthanum oxy-apatite $La_{10}AlSi_5O_{26.5}$. *J Am Ceram Soc* 2011;**94**:224–30.
25. Rietveld HM. A profile refinement method for nuclear and magnetic structures. *J Appl Crystallogr* 1969;**2**:65–71.
26. Larson AC, Dreele RBV. *General Structure Analysis System (GSAS) program. Rep. No. LA-UR-86748*. Los Alamos, CA: Los Alamos National Laboratory; 1994.
27. León-Reina L, Porras-Vázquez JM, Losilla ER, Aranda MAG. Interstitial oxide positions in oxygen-excess oxy-apatites. *Solid State Ionics* 2006;**177**:1307–15.
28. *WinDETA*. Hundsangen, Germany: Novocontrol GmbH; 1995.
29. Garmendia N, Santacruz I, Moreno R, Obieta I. Slip casting of nanozirconia/MWCNT composites using a heterocoagulation process. *J Eur Ceram Soc* 2009;**29**:1939–45.
30. Meier LP, Urech L, Gauckler LJ. Tape casting of nanocrystalline ceria gadolinia powder. *J Eur Ceram Soc* 2004;**24**:3753–8.
31. Santacruz I, Annapoorani K, Binner J. Preparation of high solids content nanozirconia suspensions. *J Am Ceram Soc* 2008;**91**:398–405.
32. Gutierrez CA, Moreno R. Tape casting of non-aqueous silicon nitride slips. *J Eur Ceram Soc* 2000;**20**:1527–37.